Diabetes, Metabolic Syndrome and Obesity

Dovepress

open access to scientific and medical research

Open Access Full Text Article

ORIGINAL RESEARCH

Electroacupuncture Reduces Inflammatory Bowel Disease in Obese Mice by Activating the Nrf2/HO-1 Signaling Pathways and Repairing the Intestinal Barrier

Yunhao Yang[1,2], Fang Pang[1–3], Min Zhou[1,2], Xiao Guo[1,2], Yan Yang[1,2], Wei Qiu[1,2], Cai Liao[1,2], Yang Chen[1,2], Chenglin Tang[1,2]

[1]College of Traditional Chinese Medicine, Chongqing Medical University, Chongqing, People's Republic of China; [2]Chongqing Key Laboratory of Traditional Chinese Medicine for Prevention and Cure of Metabolic Diseases, Chongqing, People's Republic of China; [3]Institute of Sports Biology, Shaanxi Normal University, Xi'an, Shaanxi, People's Republic of China

Correspondence: Chenglin Tang, Email tangchenglin@cqmu.edu.cn

Background: Electroacupuncture (EA) is used to treat inflammatory bowel disease (IBD). Nevertheless, the precise mechanisms by which this approach safeguards against obesity-induced intestinal barrier damage has not been fully understood.

Objective: This study aimed to assess whether EA could ameliorate intestinal barrier damage that had been reversed in a mouse model of obesity induced by a high-fat diet (HFD) and whether this repair is correlated with ferroptosis and gut microbiota enhancement.

Methods: To assess the potential of EA to prevent obesity and restore the intestinal barrier, we divided in C57BL/6J mice into two groups; one was fed with HFD and another one with a normal diet. Samples of stool, blood, fat, and intestinal epithelium were then evaluated, along with body weight.

Results: Following EA, we observed a significant reduction in body weight, fat accumulation, and serum triglyceride (TG), total cholesterol (TC), and low-density lipoprotein cholesterol (LDL-C) levels; an increase was seen in high-density lipoprotein cholesterol (HDL-C) levels. EA also activated the Nrf2 signaling pathway; upregulated the expression of GPX4, FTH1, and SLC7A11; and downregulated the expression of TFR1. In addition, the administration of EA resulted in a notable modification of the gut microbiota composition, characterized by a decrease in the Firmicutes to Bacteroidetes ratio.

Conclusion: EA had beneficial effects on weight loss and showed potential ability to repair the intestinal barrier by activating the Nrf2 signaling pathway, inhibiting intestinal inflammation and ferroptosis, and regulating the intestinal microbiota to treat IBD caused by HFD-induced obesity.

Keywords: ferroptosis, electrostimulation, acupuncture, Chinese medicine, obesity, intestinal epithelium

Introduction

Inflammatory bowel disease (IBD) is a prevalent chronic inflammatory condition characterized by recurring episodes, encompassing both Crohn's disease (CD) and ulcerative colitis(UC).[1] However, the etiology of this group of conditions is multifactorial and closely related to predisposing genes and environmental factors.[2–4] Epidemiological studies have demonstrated that a high-fat diet (HFD) plays a significant role as an external environmental factor in the development of IBD.[5,6] Therefore, the incidence of IBD has steadily increased with improvements in living lifestyle and environmental standards.[7] Previous studies have shown that HFD accelerates the progression of IBD by causing obesity, activating inflammatory responses, destroying the intestinal barrier, and altering the intestinal microbiota.[8–10] Therefore, an in-depth elucidation of its possible mechanism of action may help develop new therapeutic strategies for IBD.

Ferroptosis is a type of cell death with a unique and easily recognized mechanism that is involved in the occurrence and development of various diseases.[11,12] Studies have shown that ferroptosis is involved in the pathogenesis of IBD.[13–16] Additionally, oxidative stress mediated by ferroptosis is an important process that causes the degeneration and necrosis of

Received: 22 November 2023
Accepted: 20 January 2024
Published: 27 January 2024

Graphical Abstract

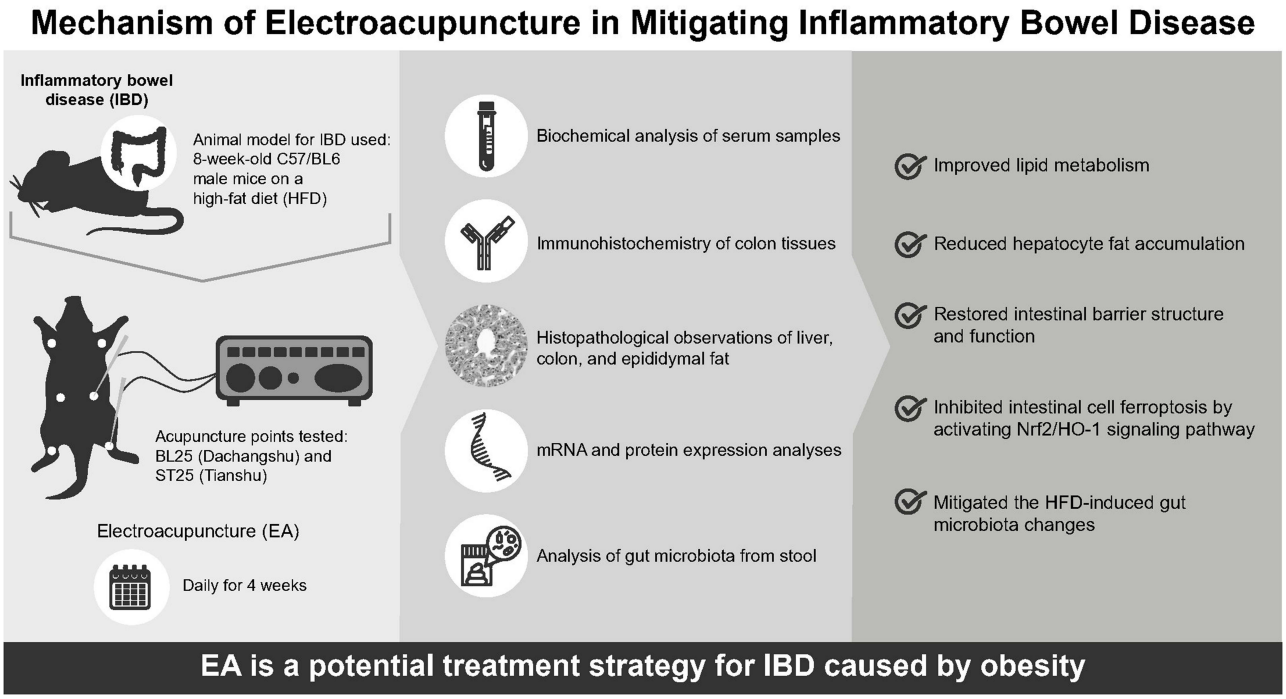

intestinal epithelial cells and plays a key role in promoting the occurrence and development of IBD.[17,18] Therefore, the inhibition of ferroptosis is a key factor in preventing the progression of IBD.

Electroacupuncture (EA) is a combination of traditional Chinese medicine therapy and modern technology. After a fine needle is inserted into an acupoint to obtain qi (arrival of qi), a trace current wave is passed through the needle, and the acupoint is stimulated by electric pulses to treat diseases. Using this method, the dual effects of electrical stimulation and acupuncture can be achieved. Earlier research has demonstrated that electroacupuncture has been extensively employed in the management of various acute and chronic illnesses, exhibiting efficacy in gastrointestinal system disorders, notably IBD.[19] The analgesic properties of electroacupuncture in IBD might be attributed to its anti-inflammatory effects induced via the cholinergic reflex as well as the hypothalamic-pituitary-adrenal axis.[20,21] Additional potential mechanisms encompass the opioid system,[22] adenosine pathway, and macrophage polarization.[23] Nevertheless, the mechanistic pathways by which electroacupuncture moderates the inflammatory response in IBD remain uncertain.

Few studies on obesity-induced colitis have been reported; therefore, the full mechanism by which EA protects against obesity-induced intestinal barrier damage remains unclear. Therefore, the aim of this study was to investigate the effect of EA on IBD in obese mice and its underlying mechanisms and to evaluate whether EA can improve IBD by inhibiting intestinal inflammation and ferroptosis and protecting the integrity of the intestinal barrier.

Materials and Methods

Animals

Eight-week-old male C57/BL6 mice, weighing between 22–26 g, were obtained from the Experimental Animal Centre of Chongqing Medical University in Chongqing, China (Certificate number: SYXK [Yu] 20220010). The mice were provided with a period of 7 days to adapt in shared plastic enclosures, ensuring suitable environmental parameters such as a temperature range of 22 ± 1°C, a humidity level of 60%, and a light/dark cycle of equal duration, each lasting 12 hours. Throughout the length of the trial, the mice were afforded unrestricted access to both food and water resources.

The animal operations conducted in this study were granted approval by the Laboratory Animal Ethical Committee of Chongqing Medical University. The committee adhered to the National Institute of Health Guidelines for the Care and Use of Laboratory Animals Reference (Number: IACUC-CQMU-2022-0017).

Following a period of acclimatization lasting 1 week, a subset of mice (n = 10) was provided with a standard diet, serving as the control (CON) group. The other mice (n = 30) were subjected to a HFD. The regular diet consisted of 15.91% (cal) fat, whereas HFD consisted of 35.92% (cal) fat. Following a period of 16 weeks during which mice were fed HFD, they were subsequently allocated randomly into 3 distinct groups: the model (MOD) group (n = 10), the electroacupuncture (EA) group (n = 10), and the sham-electroacupuncture (SEA) group (n = 10). The administration of all therapies occurred on a daily basis throughout a period of 4 weeks. The mice in the control group were provided with a standard food during the entire duration of the trial, whereas those in the remaining groups were given a HFD until the conclusion of the study.

Upon completion of the treatment, fecal samples were obtained and preserved at a temperature of −80°C. Prior to the experiment, all mice were administered pentobarbital sodium as an anesthetic following an overnight period of fasting. The ocular globes of each murine specimen were extracted, and the hemoglobin was subsequently transferred into a tube containing a procoagulant agent. Following a 30-minute incubation period at ambient temperature, the blood sample was subjected to centrifugation at a force of 1200 rpm the acceleration due to gravity for a duration of 20 minutes at a temperature of 4°C. Subsequently, the liquid portion containing suspended particles was extracted to acquire serum samples, which were subsequently preserved at a temperature of −80°C. The specimens of livers, colons, and epididymal fat were obtained and subjected to measurement of their respective weights. A segment of each liver and colon specimen was fixed with a 4% paraformaldehyde tissue fixative, while an adipose tissue fixative was applied to a segment of each epididymal fat sample. Following this, the residual tissues were submerged in liquid nitrogen and maintained at a temperature of −80°C.

Electroacupuncture

As a form of alternative medicine, acupuncture includes the penetration of particular anatomical sites with thin needles. According to earlier research investigations,[24–26] the acupuncture point BL25, also known as (Dachangshu), is situated in the waist, under the spinous process of the fourth lumbar spine, approximately 5mm away from the posterior median line. The anatomical location of ST25 (Tianshu) is in the mouse umbilicus (located in the middle of the abdomen) is 5 mm apart. Initially, the movement of the mice was constrained using a device designed to immobilize the mice, ensuring that they were in the proper body position to receive assistance. Additionally, target locations in both the EA and SEA groups were sanitized using a 75% alcohol solution. The acupuncture needles (0.16 mm × 13 mm; Zhenzheng Medical Instrument Co. LTD, Xinyang, Henan Province, China) were inserted on both sides at BL25 and ST25 to a depth of 2–3 mm. After that, the needle tips were hooked up to an electrical device. The intensity of the electrical stimulator was 0.5–1.0 mA, and its frequency was 2/15 Hz (amplitude-modulated wave). This treatment was administered for a duration of 10 minutes per day in the EA group. The SEA group of mice underwent bilateral needle insertion at the sham acupoints to a depth of 2–3mm. Subsequently, the needle handles were affixed to an electrical device; however, no electrical current stimulation was delivered. While the other groups did not receive acupuncture or electrical stimulation, the mice in these groups were nonetheless subjected to fixtures that were comparable to those used in the EA group.

Biochemical Testing

Triglycerides (TG), total cholesterol (TC), low-density lipoprotein cholesterol (LDL-C) and high-density lipoprotein cholesterol (HDL-C), aspartate aminotransferase (AST), and alanine aminotransferase (ALT) serum concentrations, as well as TC and TG liver tissue concentrations, were measured using commercially available kits (Nanjing Jiancheng Bioengineering Institute in Jiangsu, China).

ELISA Analysis

The levels of inflammatory cytokines, specifically interleukin IL-1β, IL-10, IL-6, and tumor necrosis factor (TNF)-α in the serum were measured using mouse-specific enzyme-linked immunosorbent assay (ELISA) kits. The procedures were executed in accordance with the guidelines provided by the manufacturer. The samples were loaded into the corresponding wells of the micro-ELISA strip-plate. In each sample, specific antibodies coupled with horseradish peroxidase were introduced for incubation. Following this, coloration was induced by the application of chromogen solutions A and B. To terminate the reaction, a stop solution was introduced, which produced a visible color change from blue to yellow. The measurement of optical density (OD) was conducted using a microplate spectrophotometer at a specific wavelength of 450 nm. Each sample was analyzed in two replicates, and the mean concentrations of antigens per gram of protein were calculated and presented as picograms.

Transmission Electron Microscopy

After three rinses with a 0.1 mol/L phosphoric acid solution, the colons were fixed for three times with a 1% osmic acid solution. Subsequently, they were dehydrated using graded alcohol and acetone solutions at a temperature of 4°C, and once more dehydrated with 100% acetone at ambient temperature. Embedded tissues were subjected to curing in an oven. The tissues were sectioned at a 70-nm thickness using an ultrathin slicer. To visualize Tight junction in the intestinal tract barrier, the sections were stained with 3% uranium acetate and lead citrate.

Histopathological Observations

Each mouse's epididymal fat, colon, and liver were fixed separately in 4% buffered formalin, a special fixative for fat, and 4% epididymal fat, respectively. To perform hematoxylin and eosin (H&E) and oil red staining, paraffin-embedded fixed liver tissues were embedded in an optimal cutting temperature (OCT) embedding agent. Subsequently, the sections were sectioned at a thickness of 4-μm. H&E staining was also performed on epididymal adipose and colon tissues to verify the dimensions of the adipocytes. The slides were subsequently subjected to light microscopy.

Immunohistochemistry of Colon Tissues

To rehydrate paraffin sections of colon samples, a series of different ethanol concentrations were progressively added after dewaxed with xylene. Following this, a microwave antigen recovery technique was employed to pre-treat the slides, followed by blocking with 5% bovine serum albumin (BSA). Primary antibodies (OCLN Polyclonal Antibody (Occludin, 1:1000, No. AF10472, AiFang]; Tight junction protein ZO-1 (ZO-1, 1:1000, No. AF09017, AiFang) were used to incubate sections at 4°C for an overnight period. Following three washes with phosphate-buffered saline (PBS), the tissues were incubated for 50 minutes at room temperature with a secondary antibody. Following three additional washes with PBS, the sections were processed with 3.3′diaminobenzidine (DAB) and stained with hematoxylin. Following dehydration and fixation, a microscope was used to observe the stained tissues. Subsequently, suitable images were obtained and examined.

Immunofluorescence Location Examination

Following the dewaxing process, the paraffin sections of the small intestine were subjected to repair, permeation, and subsequent sealing. The paraffin sections were subsequently subjected to incubation at room temperature with the appropriate concentration of primary antibodies. These included the nuclear factor erythroid 2-related factor 2 (Nrf2) antibody (1:1000, No.AF02883, AiFang) and the heme oxygenase-1 (HO-1) polyclonal antibody (1:1000, No. A1346, Abclonal). The incubation was carried out in a wet box for a duration of 1 hour. Following three washes with PBS, paraffin sections were subjected to incubation at 22–26°C using Goat Anti-Mouse IgG H&L (Alexa Fluor® 488) (1:1000, Catalog No. ab150113; Abcam) as the secondary antibody for a duration of 1 hour. The nuclei were subjected to staining using 4′,6-diamidine-2′-phenylindole dihydrochloride (DAPI, 1:1000, No. D9542, SIGMA), while the sections were stained using a phalloidin solution (YF594-Phalloidin, 1:1000, No. YP0052, Us) in a light-restricted environment. The stained samples were promptly seen using inverted fluorescence microscopy.

Quantitative Real-Time PCR

The AG RNAex Pro Reagent (code: AG 21102) was utilized to extract total RNA from 50 mg of mouse colon tissue, following the guidelines provided by the manufacturer. The Evo M-MLV RT Premix for qPCR (code: AG11706) was employed as a reverse transcription reagent to convert total RNA into complementary DNA (cDNA) for the purpose of conducting a quantitative real-time PCR (qRT-PCR) experiment. This was done in accordance with the SYBR® Green Premix Pro Taq HS qPCR kit (code: AG11701). Moreover, the mRNA expression levels of each sample were standardized by normalizing them to the expression levels of glyceraldehyde-3-phosphate dehydrogenase (GAPDH). The cycling conditions utilized in this study were as follows: an initial denaturation step at a temperature of 95°C for a duration of 30 seconds, followed by further cycling steps at temperatures of 94°C for 5 seconds, 60°C for 15 seconds, and 72°C for 10 seconds. The CFX Connect instrument, manufactured by Bio-Rad and located at 1000 Alfred Nobel Drive, Hercules, CA 94547, USA, was employed for this purpose. The data obtained were analyzed utilizing the $2^{-\Delta\Delta Ct}$ methodology. The primers employed for quantitative reverse transcription polymerase chain reaction (qRT-PCR) are presented in Table 1.

Western Blotting Analysis

The analysis of protein expression levels was conducted using Western blotting. The proteins present in the tissue were isolated and lysed by employing the RIPA buffer. To achieve this objective, a quantity of proteins found in tissues lysates was initially subjected to separation using sodium-dodecyl-sulfate-polyacrylamide gel electrophoresis (SDS-PAGE), followed by subsequent transfer onto a polyvinylidene difluoride (PVDF) membrane. The subsequent step involved incubating the protein bands with the primary antibodies listed below: Nrf2 (1:1000, No.AF02883, AiFang), HO-1 (1:1000, No. A1346, Abclonal), Occludin (1:1000, No. AF10472, AiFang), ZO-1 (1:1000, No. AF09017, AiFang), TFR1 (1:1000, No. ab1086, Abcam), FTH1 (1:1000, No. 3998S, CST), SLC7A11 (1:1000, No. 98051S, CST), GPX4 (1:1000, No. 52455S, CST). Furthermore, β-actin (1:1000, No. 2118S, CST) was used as the loading control. Finally, the membranes were scanned by Image studio. The grey values of each band were calculated using Image J software.

Stool Analysis of Gut Microbiota

Samples were expeditiously frozen by immersing them in liquid nitrogen and subsequently stored at a temperature of −80°C. The PCR procedure for amplifying the V3–V4 region of the bacterial 16S rRNA genes involved the utilization of forward primer 338F (5'-ACTCCTACGGGAGGCAGCA-3') and reverse primer 806R (5'-GGACTACHVGGGTWTCTAAT-3'). In the primers utilized for multiplex sequencing, sample-specific 7-bp barcodes were integrated. 5.25 μL of fast pfu DNAPolymerase (5U/μL), 2 μL (2.5 mM) of dNTPs, 1 μL (10uM) of forward and reverse primer, 1 μL of DNATemplate, and 14.75 μL of ddH2O comprised the PCR components. Following an initial denaturation period of 5 minutes at 98°C, the material underwent 25 cycles of denaturation for 30 seconds at 98°C, annealing for 30 seconds at 53°C, and extension for 45 seconds at 72°C, culminating in a final extension of 5 minutes at 72°C. The VazymeVAHTSTM DNA Clean Beads (Vazyme, Nanjing, China) were utilized to purify the PCR amplicons, which were subsequently quantified employing the Quant-iT PicoGreendsDNA Assay Kit (Invitrogen, Carlsbad, CA, USA). Following the individual quantification phase, amplicons were pooled in equal quantities and subjected to pair-end 2250 bp sequencing utilizing the MiSeq Reagent Kit v3 and the Illumina MiSeqplatform.

Table 1 Sequences and Product Length of Primers Used

Gene	Forward Primer	Reverse Primer
GPX4	CCCGATATGCTGAGTGTGGTTTA	TTCTTGATTACTTCCTGGCTCCTG
FTH1	GGCTGAATGCAATGGAGTGTG	GTGGTCACCCAGTTCTTTAATGG
TFR1	GTTTCTGCCAGCCCCTTATTAT	GCAAGGAAAGGATATGCAGCA
Slc7a11	CCCTGGCATTTGGACGCTAC	CTCCAGCTGACACTCGTGCTATTTA

Statistical Analysis

The data are presented as the mean ± standard error of the mean (mean ± SEM) from three separate studies. A one-way analysis of variance (ANOVA) was conducted, followed by a post-hoc multiple comparison test, to assess and evaluate significant variations across various groups. In the context of statistical analysis, a significance level of $p < 0.05$ was deemed to indicate statistical significance, while a significance level of $p < 0.01$ was regarded as indicative of a high degree of statistical significance.

Results

EA Reduce the Obesity Traits in HFD-Induced Obese Mice

At the initiation of the trial, the weights of the mice in each group were roughly equivalent. Following a duration of 16 weeks, it was observed that the HFD-fed mice exhibited a higher average weight growth compared to the CON mice, thus demonstrating the successful establishment of the model (Figure 1A). After 4 weeks treatment, it was observed that the increase in body weight was comparatively smaller in the EA group as compared to the MOD group, as depicted in Figure 1B. The findings of this study demonstrate that the administration of EA had a substantial impact on mitigating weight gain and reducing fat buildup in mice that were fed with HFD. The HFD resulted in elevated blood lipid levels in obese mice, as evidenced by a notable rise in serum levels of TC, TG, and LDL-C, accompanied by a decrease in serum levels of HDL-C, when compared to the CON group (Figure 1E–H). The administration of EA resulted in a considerable decrease in the serum levels of TC, TG, and LDL-C, while simultaneously causing a significant increase in the serum levels of HDL-C in mice that were fed with HFD (Figure 1E–H). In addition, compared with the CON group, the volume of epididymal fat in the MOD group was significantly increased. HE staining showed that the volume of adipocytes was larger, the content of vacuoles in cells was increased, and the cell boundary was not clear and the cells were arranged in disorder. In the EA group, the epididymal adipose tissue was significantly reduced, the content of vacuoles in the epididymal adipocytes was reduced, and the cells were arranged neatly with clear cell boundaries. There was no significant difference between the SEA and MOD groups (Figure 1C and D). The findings of this study demonstrate that EA intervention led to a considerable improvement in blood lipid levels in mice that were created to be obese through the HFD.

Effects of EA Treatment on Hepatic Steatosis in HFD-Induced Obese Mice

HE and Oil Red O staining revealed pronounced lipid deposition in the liver of mice, accompanied by disorganized hepatocyte structure, varying sizes of droplets, and alterations in the MOD group. Notably, the MOD group exhibited significantly greater abnormal lipid accumulation in the liver compared to the CON group, the group treated with EA had a significant decrease in hepatic lipid accumulation, as depicted in Figure 2A–C. In accordance with the Elisa results, the hepatic concentrations of TG and TC in mice from the MOD group exhibited a statistically significant elevation compared to those from the CON group. The addition of EA resulted in a considerable decrease in hepatic levels of TG and TC, as seen in Figure 2D and E. Furthermore, the MOD group exhibited a notable elevation in blood levels of ALT and AST in comparison to the CON group. After the treatment, there was a notable decrease in the serum levels of ALT and AST (Figure 2F and G).

EA Influenced Colonic Inflammation and Intestinal Barrier Integrity

For HE staining, Compared with the CON group, the MOD group had increased inflammatory cell infiltration, epithelial loss, crypt structure destruction, and goblet cells reduction. Compared with the MOD group, the colonic inflammatory pathology of the EA group was better improved, but there was no significant improvement in the SEA group (Figure 3A).

The ultrastructure of colonic mucosa was observed by transmission electron microscope. In the CON group, the ultrastructure of intestinal tight junctions was intact and the electron density was high. The tight junction structure of the MOD group was loose and the electron density was low. The tight junction structure was restored in the EA group, while the results in the SEA group and the model group were similar (Figure 3B).

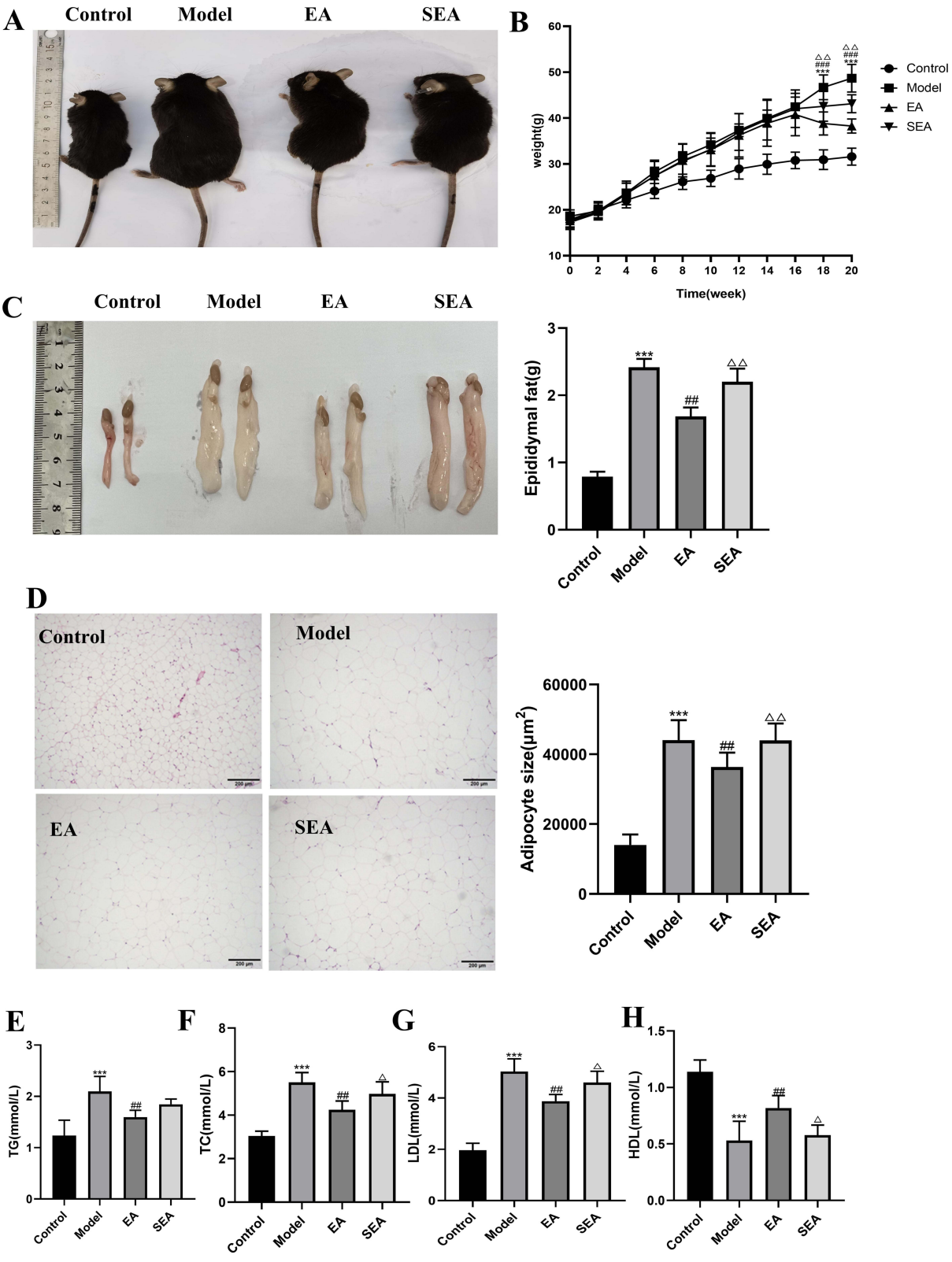

Figure 1 EA reduced body weight and fat deposition (**A**) Appearance of mice. (**B**) Body weight gain. (**C**) Appearance of epididymal fat. (**D**) HE staining of epididymal adipose tissue and Epididymal adipocyte area (scale bar = 200 μm). (**E**) Serum TC. (**F**) Serum TG. (**G**) Serum LDL-C. (**H**) Serum HDL-C. n= 6, values are mean ± SEM),*** $p < 0.001$ (Control vs Model); $^{\#\#}$ $p < 0.01$,$^{\#\#\#}$ $p < 0.001$ (Model vs EA); $^{\Delta}$ $p < 0.05$, $^{\Delta\Delta}$ $p < 0.01$ (EA vs SEA).

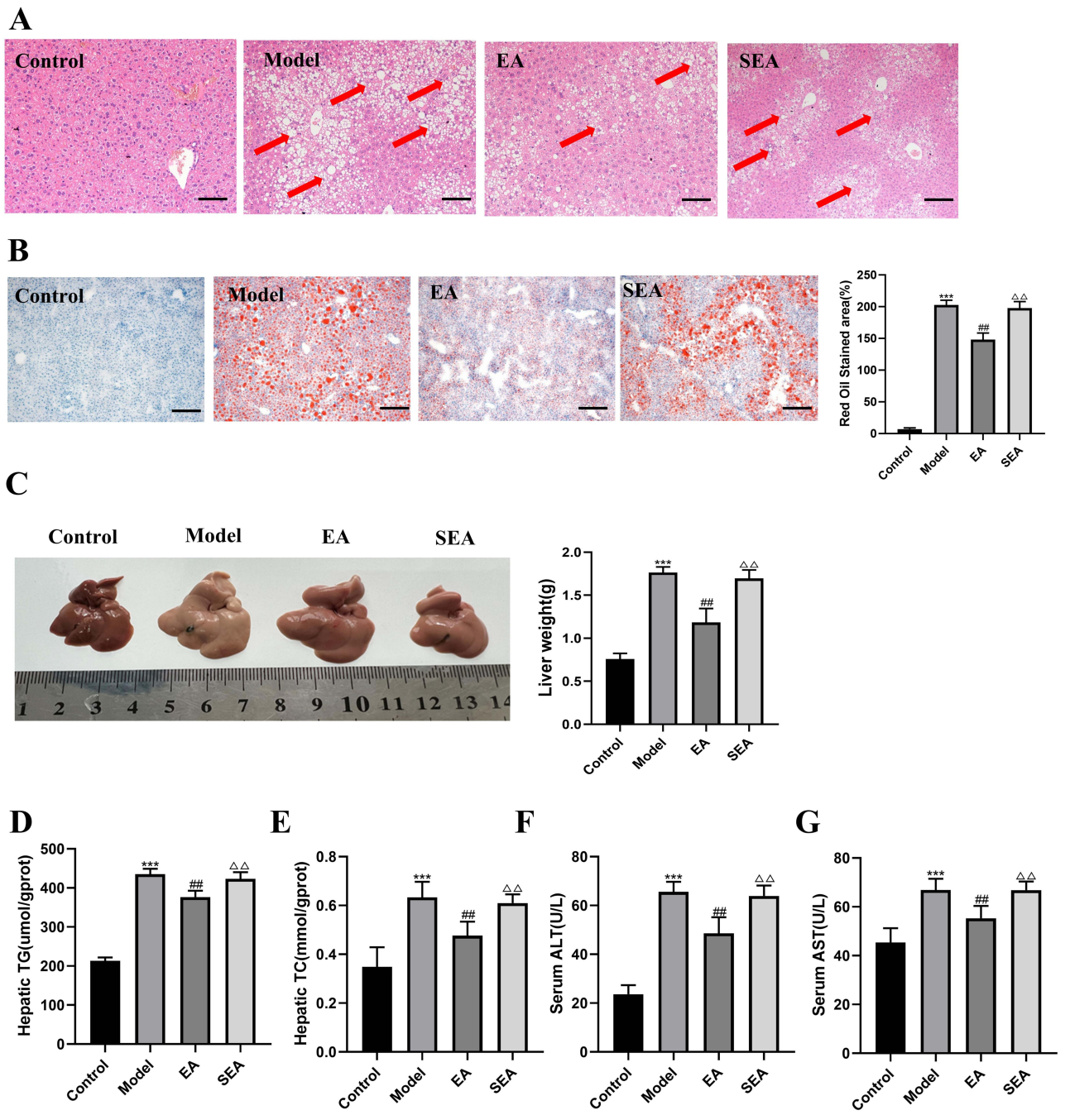

Figure 2 EA improves liver steatosis and liver function in mice (**A**) H E staining of liver tissue (scale bar = 200 μm). The red arrows indicate typical hepatic inflammation. (**B**) Liver tissue stained with Oil Red O (scale bar = 200 μm). (**C**) Morphology of liver. (**D**) Hepatic TG. (**E**) Hepatic TC. (**F**) Serum ALT. (**G**) Serum AST. n= 6, values are mean ± SEM; *** $p < 0.001$ (Control vs Model); ## $p < 0.01$ (Model vs EA); △△ $p < 0.01$ (EA vs SEA).

As depicted in Figure 3C, the length of the colon was found to be shorter in the MOD group than in the CON group and the EA group. The ELISA levels of TNF-α, IL-6 and IL-1β showed a decreasing trend in the EA group, compared with those in the MOD group. However, the EA group exhibited higher colonic IL-10 ELISA expression than the MOD group (Figure 3D–G).

Figure 3F clearly shows that the protein expression levels of ZO-1 and Occludin were higher in the EA group than in the MOD group. Similarly, immunohistochemistry staining and Western blotting revealed that the distribution of ZO-1 and Occludin in the colon was enhanced in the EA group (Figure 3H and I).

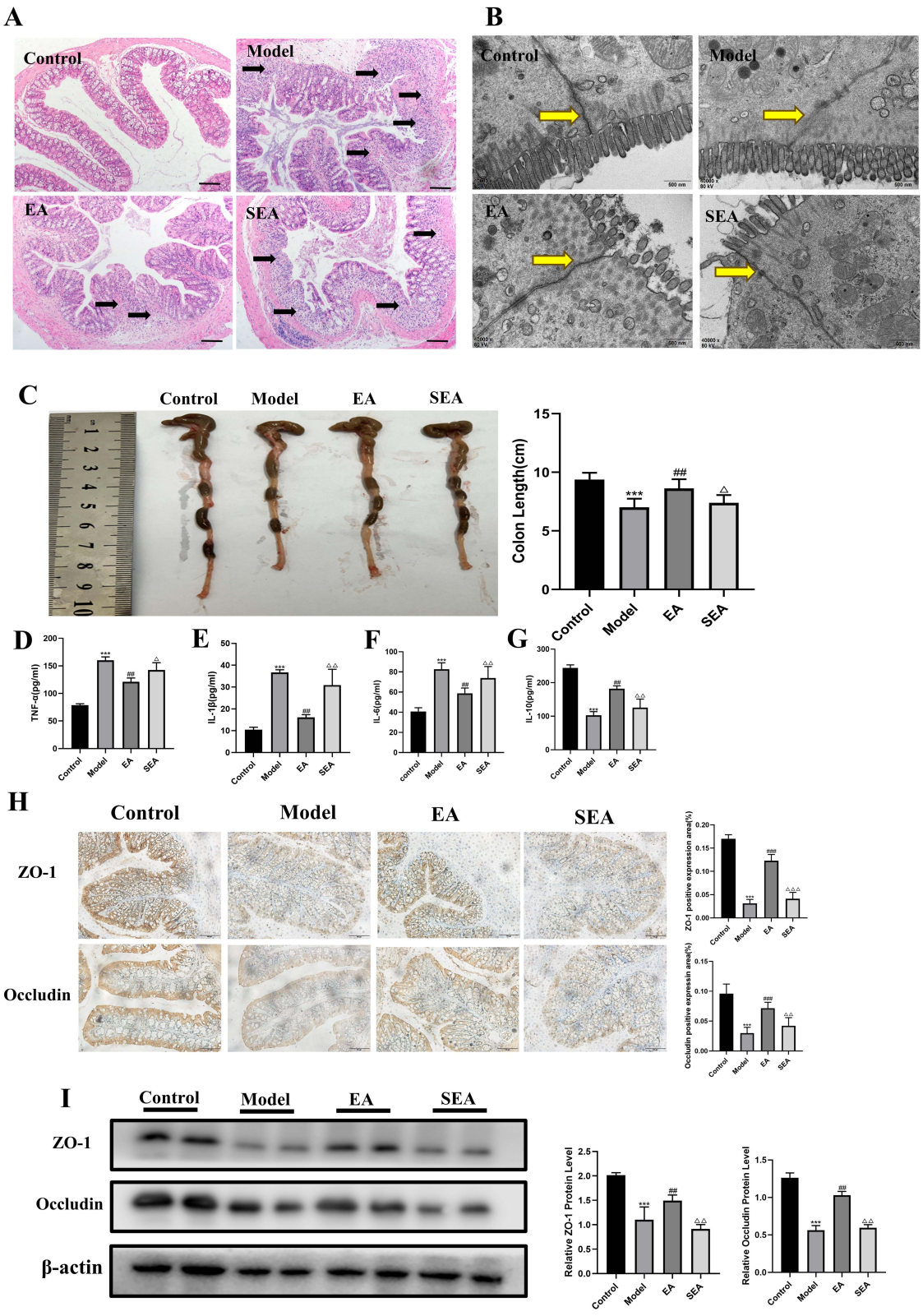

Figure 3 EA improves colonic inflammation and intestinal barrier tight junction structure in obese mice (**A**) HE staining of colon tissue (scale bar =100 μm). Black arrows indicate typical intestinal inflammation. (**B**) Electron microscopy of colon tissue (scale bar =40000 μm), The site indicated by the yellow arrow is the tight junction structure. (**C**) Colon length of mice in each group(**D**)Colonic TNF-α. (**E**) Colonic IL-1β. (**F**) Colonic IL-6. (**G**) Colonic IL-10. (**H**) Immunohistochemical analysis of the expression of individual proteins (scale bar = 100 μm). (**I**) Immunoblot analysis of individual protein expression (β-actin as internal reference). n= 6, values are mean ± SEM; *** $p < 0.001$ (Control vs Model); ## $p < 0.01$, ### $p < 0.001$ (Model vs EA); $^{\Delta}$ $p < 0.05$, $^{\Delta\Delta}$ $p < 0.01$, $^{\Delta\Delta\Delta}$ $p < 0.001$ (EA vs SEA).

Effects of EA Treatment on the Nrf2/HO-1 Signaling Pathway in HFD-Induced Obese Mice

Ferroptosis has been implicated in the Nrf2/HO-1 signaling pathway, anti-inflammatory and anti- antioxidant effects of EA are mediated through the Nrf2/HO-1 signaling pathway. Immunofluorescence results showed that the fluorescence intensity of Nrf2 and HO-1 in intestinal tissue of MOD group was significantly lower than that of CON group, suggesting that this pathway may be inhibited. The results of SEA group were similar to those of MOD group. However, the fluorescence intensity of Nrf2 and HO-1 in the EA group was significantly increased, suggesting that EA may activate the Nrf2 pathway (Figure 4A). This result is also consistent with Western blotting results (Figure 4B).

EA Inhibited Ferroptosis in HFD-Induced Obese Mice

To gain mechanistic insights into the therapeutic effects of EA, ferroptosis this process was examined in HFD-induced obese mice. TFR1, GPX4, FTH1, and SLC7A11 were surrogate markers of ferroptosis.[27–31] As shown in Figure 5AB, HFD led to increase in the expression of TFR1. EA treatment decreased TFR1 expression; moreover, the EA groups had elevated levels of GPX4, FTH1, and SLC7A11 in the colons of mice, compared to the MOD group (Figure 5A and B). Collectively, these findings suggest that EA inhibits ferroptosis in experimental models of colitis.

EA Reverses HFD-Induced Obese Mice Gut Dysbiosis

The data presented in this study demonstrate a decrease in the richness of intestinal flora in mice fed with HFD. The observed values of the species in the MOD group exhibited a statistically significant decrease compared to the CON group, suggesting a notable difference between the two groups. In contrast, the intervention conducted by EA resulted in an augmentation of the variety observed in the microbiota of mice. The α-diversity in mice from the EA group exhibited an upregulation when compared to that in mice from the MOD group (Figure 6A). A statistically significant increase in the Simpson index was observed in the HFD group as opposed to the control group. To facilitate a more comprehensive comparison of the structural alterations in the microbial communities of mice, a principal coordinates analysis (PCoA) was conducted on the abundances of operational taxonomic units (OTUs) derived from the samples obtained from three groups. The PCoA map illustrates the degree of similarity in mouse microorganisms between the CON and EA groups. Conversely, the data from the HFD and EA groups exhibit a spatial separation, with each group occupying distinct regions within the diagram (Figure 6B and C). Except for unidentified-Bacteria, the taxonomic profiling analysis revealed that the gut microbiota in mice was primarily characterized by the presence of Firmicutes and Bacteroidetes at the phylum level (Figure 6D). At the phylum level, a notable rise in the relative abundance of Firmicutes was seen in the model group in comparison to the control group (Figure 6F). Conversely, there was a significant decrease in the relative abundance of Bacteroidetes (Figure 6E), resulting in a significant increase in the Firmicutes to Bacteroidetes ratio (F/B) (Figure 6G). In comparison to the model group, the EA group exhibited a notable rise in the relative abundance of Bacteroidetes, and there was a significant drop in the relative abundance of the F/B ratio.

Discussion

Electroacupuncture, a therapeutic technique derived from the ancient practice of acupuncture in traditional Chinese medicine, has shown great potential in improving gastrointestinal motility in animal models.[26,32] However, there is currently no conclusive evidence supporting its effectiveness in managing inflammatory bowel disease. Previous studies have suggested that EA can have beneficial effects on colitis.[33,34] This study aimed to showcase EA's effects on obese IBD mice, encompassing weight reduction, diminished fat accumulation, and inflammation mitigation. Additionally, EA exhibited inhibitory effects on colonic ferroptosis in IBD-afflicted mice, concurrently activating the Nrf2/HO-2 signaling pathway.

Obesity is a prevailing issue among individuals with IBD, particularly in emerging developed nations. Multiple epidemiological investigations have demonstrated that around 15% to 40% of IBD patients exhibit obesity, and there is a potential linkage between obesity and the development of IBD.[35] Our study's findings indicate that the EA group of mice had diminished blood lipids, reduced body weight, and decreased fat accumulation in the liver and epididymis when compared to the MOD group. These outcomes suggest that EA intervention has the capability to ameliorate abnormal fat

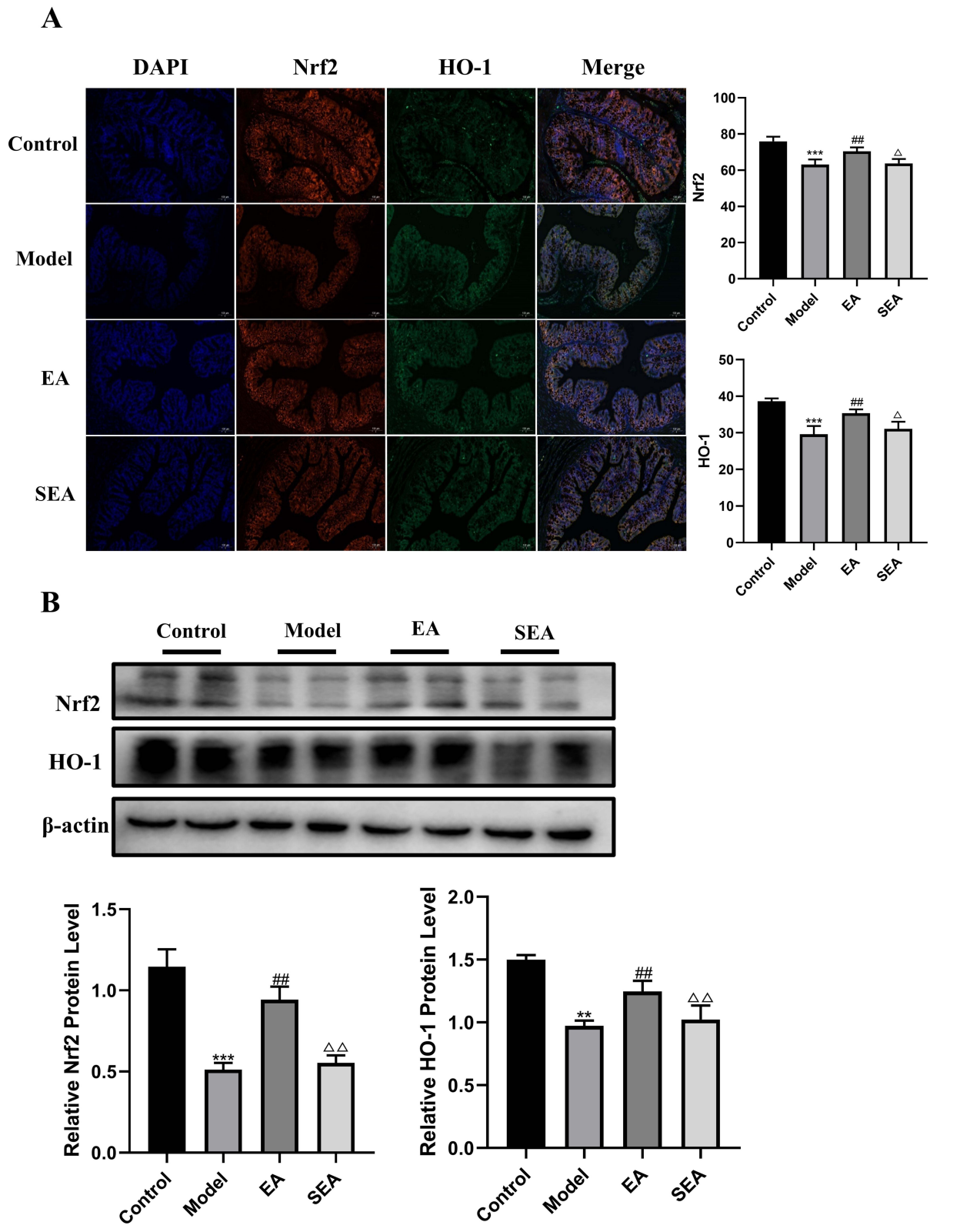

Figure 4 The effects of EA on the Nrf2/HO-1 signaling pathway in COLON tissue. (**A**) Immunofluorescence of colon tissue (scale bar = 100 μm). (**B**) Immunoblot analysis of individual protein expression (β-actin as internal reference). n= 4, values are mean ± SEM; ** $p < 0.01$,*** $p < 0.001$ (Control vs Model); $^{\#\#}$ $p < 0.01$ (Model vs EA); $^{\Delta}$ $p < 0.05$, $^{\Delta\Delta}$ $p < 0.01$ (EA vs SEA).

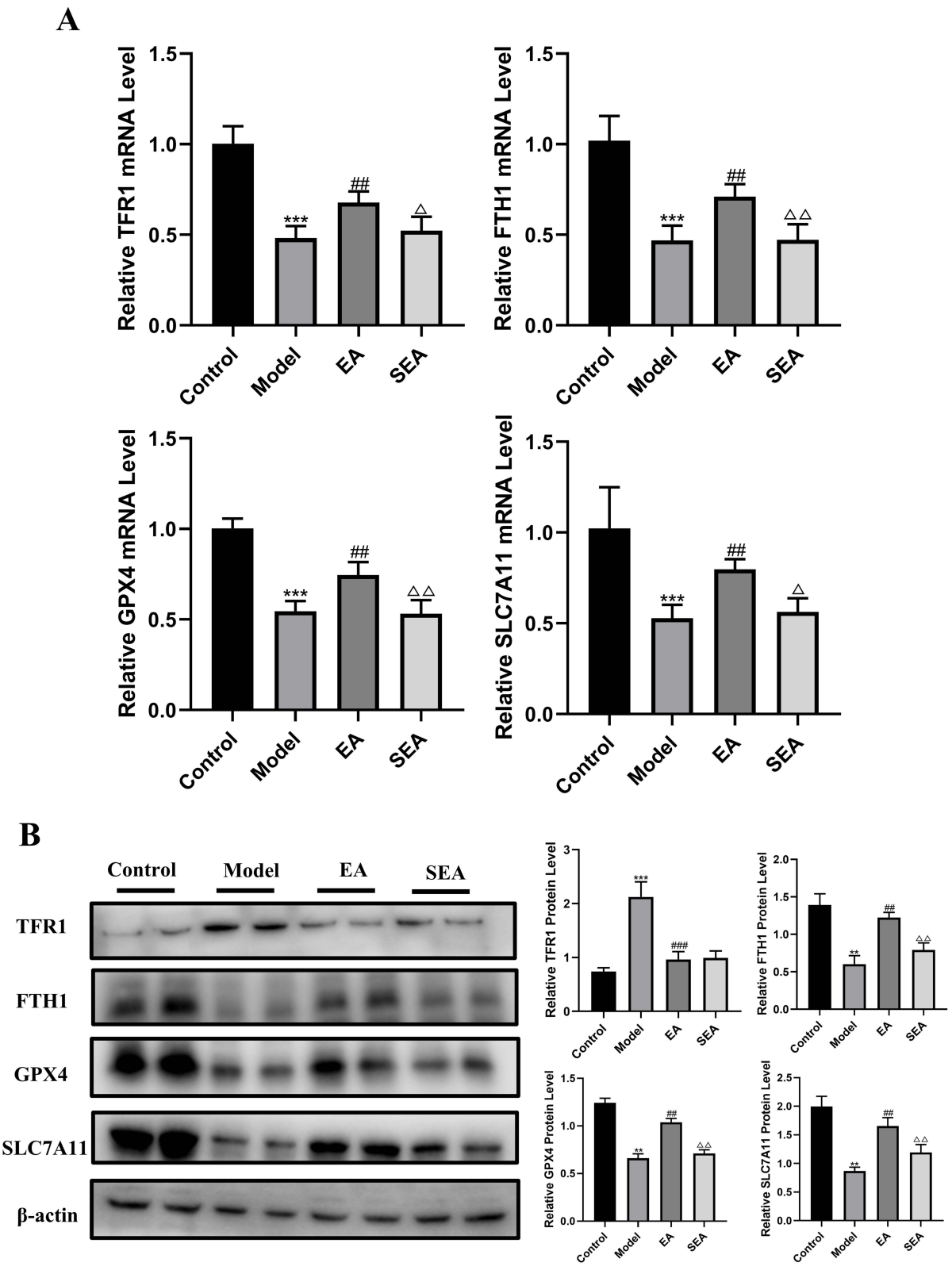

Figure 5 EA ameliorated IBD in obese mice by inhibiting ferroptosis in the gut Gene and protein levels were verified. (**A**) Gene expression (GAPDH as internal reference). (**B**) Protein expression (β-actin as internal reference). n = 6, values are mean ± SEM; ** $p < 0.01$,*** $p < 0.001$ (Control vs Model); ## $p < 0.01$, #### $p < 0.01$ (Model vs EA); Δ $p < 0.05$, ΔΔ $p < 0.01$ (EA vs SEA).

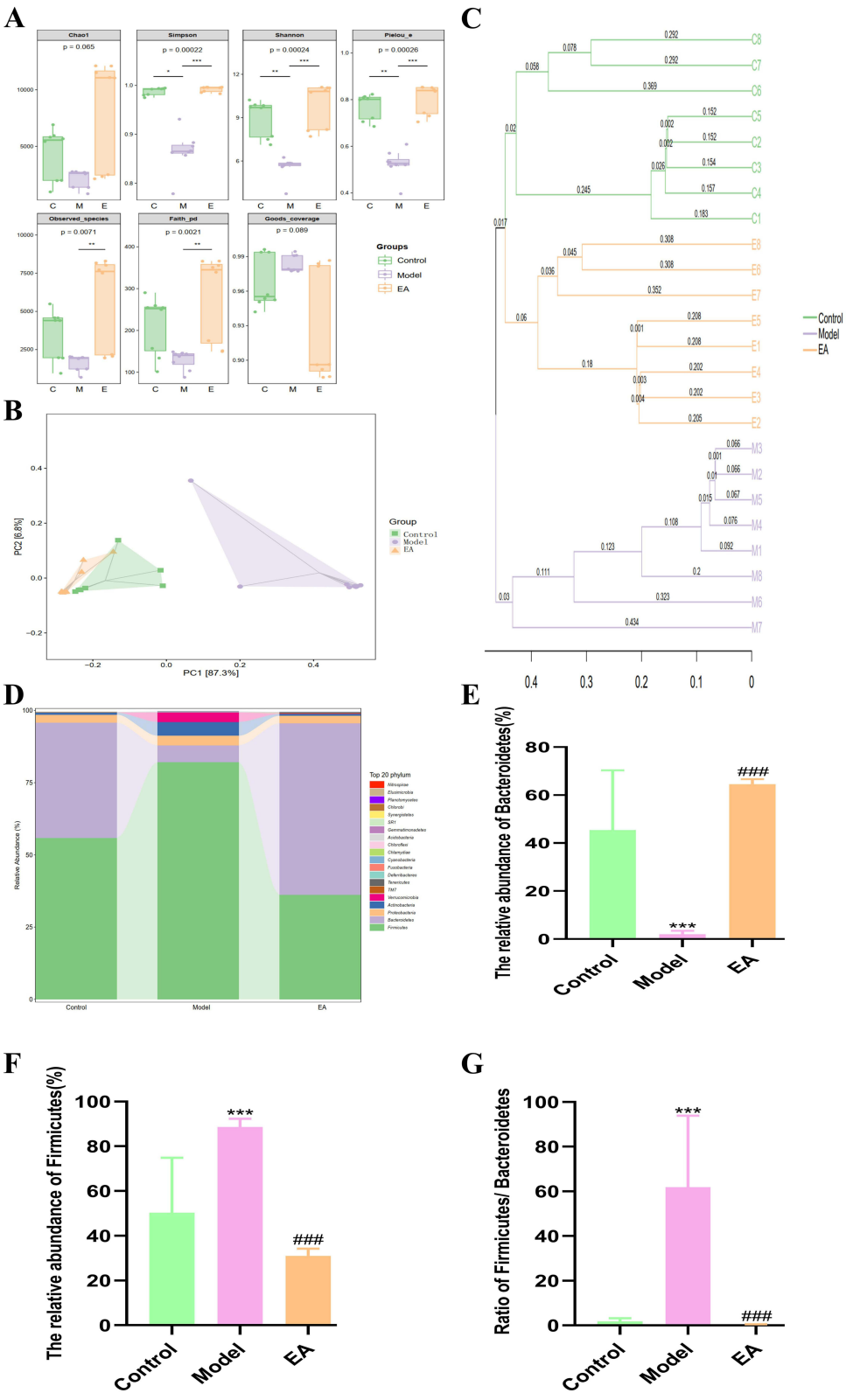

Figure 6 Effect of EA on gut microbiota of mice with high-fat diet (**A**) Alpha diversity index. (**B**) PCoA analysis. (**C**) UPGMA analysis. (**D**) Species group at phylum level. (**E**) The relative abundance of Bacteroidetes.(**F**) The relative abundance of Firmicutes (**G**)The ratio of Firmicutes to Bacteroidetes. n = 8, values are mean ± SEM; * (Control vs Model), *p < 0.05, ** p < 0.01,*** p < 0.001; ### p < 0.01 (Model vs EA).

https://doi.org/10.2147/DMSO.S449112 DovePress

accumulation and lipid metabolism disorders caused by a high-fat diet. Some researchers have established that acupuncture point ST25 and BL25 can effectively regulate high-density lipoprotein levels, triglyceride levels, and appetite scores. The mechanism of action for ST25 and BL25 involve the production of superoxide, which induces lipolysis,[36] and our results further support this theory. In addition to this, obesity is also associated with an imbalance in gut microbiota, as an inequity between energy intake and expenditure promotes the prevalence of pathogenic bacteria.[37] In our investigation, we observed that mice in the MOD group experienced gut dysbiosis, which was mitigated following administration of EA. These findings not only affirm the correlation between gut microbiota and obesity but also suggest that acupuncture point ST25 and BL25 have the potential to improve gut dysbiosis.

In our study, we observed that EA ameliorated colon length shortening and tissue damage in IBD-afflicted mice. Pro-inflammatory cytokines like IL-1β, IL-6, and TNF-α play pivotal roles in initiating intestinal inflammation in IBD.[38] Previous research has highlighted that ST25 acupuncture diminishes nuclear factor kappa beta levels, thereby curtailing the transcription of proinflammatory cytokines such as TNF-α and IL-6.[39] Our findings corroborated this observation, as EA effectively counteracted the HFD-induced surge in pro-inflammatory cytokines. Additionally, EA's impact on IBD development involved fortifying the integrity of the intestinal epithelial barrier. Assessment of tight junction protein expression revealed that EA reversed the HFD-induced decline in ZO-1 and Occludin levels in mice. These results underscore EA's potential to mitigate inflammation, restore epithelial barrier integrity, and alleviate symptoms associated with IBD.

Nrf2, a vital regulator of cellular antioxidant responses, plays a crucial role in governing ferroptosis by controlling the expression of ferroptosis-related genes like FTH1, TFR1, HO-1, SLC7A11, and GPX4.[40] Our investigation revealed diminished levels of Nrf2 and HO-1 in the MOD group's mice, suggesting a potential impairment of the Nrf2/HO-1 signaling pathway in IBD. Notably, EA treatment increased Nrf2 and HO-1 levels, indicating a promising restoration of this pathway through stimulation of the ST25 and BL25 acupuncture points

IBD-afflicted intestinal tissues from patients and animal models exhibit characteristic features of ferroptosis,[41–43] closely linked with intestinal epithelial cell death.[44] Dysregulation of key ferroptosis-related genes significantly influences the progression, severity, and incidence of experimental colitis in mice.[45,46] GPX4 is an antioxidant protein that promotes the decomposition of hydrogen peroxide and lipid peroxides, removes excess ROS accumulated in the body, and protects cells from oxidative damage. It is considered the core factor regulating ferroptosis and can, therefore, be used as an important indicator of ferroptosis. SLC7A11 is mainly used to synthesize the intracellular antioxidant protein, GSH, which cooperates with GPX4 to play an antioxidant role and is an important regulator of ferroptosis.[47,48] Lei et al[49] showed that radiotherapy could inhibit SLC7A11 protein expression, weaken the antioxidant effect of GPX4, and trigger ferroptosis. TFR1 is a transmembrane transport protein that control the cellular uptake of iron. Studies have found that TFR1 is closely related to ferroptosis and that increased expression of TFR1 is a marker of ferroptosis.[50] In our study, EA treatment in colitis mice significantly down-regulated the pro-ferroptosis gene TFR1 and up-regulated the inhibitory ferroptosis genes FTH1, GXP4, and SLC7A11. These findings indicate EA's potential to mitigate excessive intestinal ferroptosis in IBD mice.

The symbiotic relationship between intestinal epithelial cells and the vast array of intestinal bacteria is widely recognized for its pivotal role in host nutrition and metabolic functions.[51] This symbiosis is integral in preserving the structural integrity of the intestinal mucosal barrier and regulating immune responses.[52] Alterations in the microbiota composition can exacerbate colitis-related conditions by fostering chronic inflammation.[53,54] Our study data demonstrate a reduction in intestinal microbiota richness in mice fed a high-fat diet. Conversely, EA intervention led to increased diversity in the mouse microbiota, notably elevating the relative abundance of the phylum Bacteroidetes. These findings highlight that EA's protective effects are closely associated with the restoration of intestinal microbiota proportions in HFD-induced IBD.

There are several limitations associated with this investigation. Firstly, the construction of Nrf2 knockout mice was not carried out, which remains a focus of our future research. Subsequent endeavors aim to construct Nrf2 knockout mice to validate if Nrf2 deficiency can spontaneously induce IBD and to evaluate the effectiveness of EA re-administration. Additionally, further verification is crucial to establish a specific correlation between the ST25 and BL25 acupuncture point, ferroptosis, and the Nrf2/HO-1 signaling pathway. Finally, it's imperative to confirm the impact of the ST25 and BL25 acupuncture point on the intestinal flora and explore any explicit regulation of bacterial phyla.

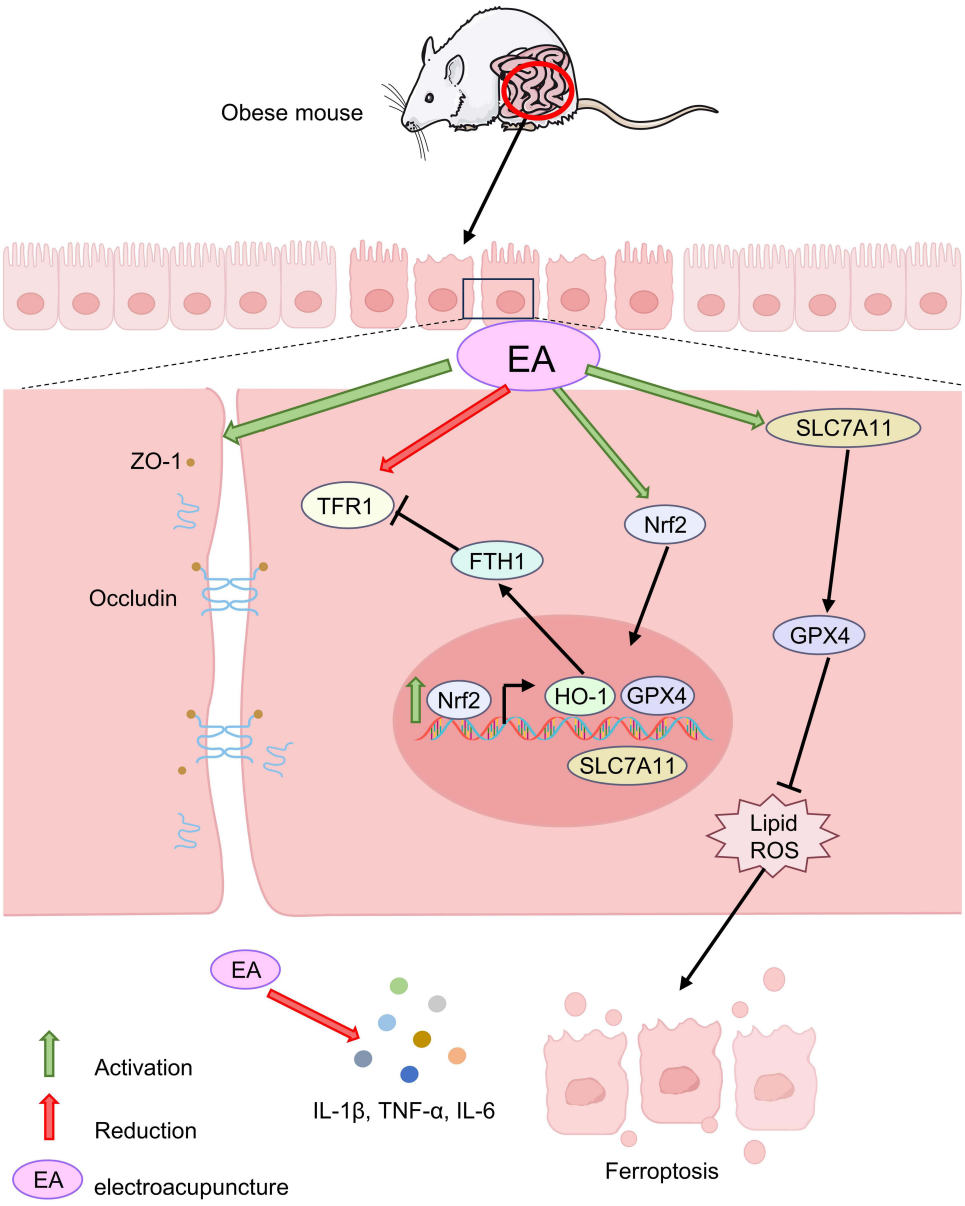

Figure 7 Diagrammatic representation for the mechanism of current explored study.

Conclusion

In the present study, HFD-induced obesity in mice mimicked the features of human obesity and resulted in increased mesenteric fat deposition, development of colonic inflammation. EA can alleviate the development of IBD by reducing body weight, reducing the inflammatory response, and inhibiting ferroptosis in mice, providing a new strategy for the treatment of IBD caused by obesity using traditional Chinese medicine, as shown in Figure 7.

Institutional Review Board Statement

This study protocol was approved by the Ethics Committee of Chongqing Medical University (Reference Number: IACUC-CQMU-2022-0017).

Author Contributions

All authors made a significant contribution to the work reported, whether that is in the conception, study design, execution, acquisition of data, analysis and interpretation, or in all these areas; took part in drafting, revising or critically reviewing the article; gave final approval of the version to be published; have agreed on the journal to which the article has been submitted; and agree to be accountable for all aspects of the work.

Funding

This study was supported by the Key Discipline Construction Project of Acupuncture Moxi-bustion and Massage of Chongqing Health Commission (472020320220021), College of Traditional Chinese Medicine of Chongqing Medical University (No: 2021-ZDXK-DB07), Joint Project of Chongqing Health and Family Planning Commission and Science and Technology Commission (No: ZY201801007), and Chongqing Yuzhong District Science and Technology Plan Project (No: 20200116).

Disclosure

The authors declare no conflicts of interest in this work.

References

1. Wirtz S, Popp V, Kindermann M, et al. Chemically induced mouse models of acute and chronic intestinal inflammation. *Nature Protocols*. 2017;12(7):p. 1295–1309. doi:10.1038/nprot.2017.044
2. Ananthakrishnan AN, Bernstein CN, Iliopoulos D, et al. Environmental triggers in IBD: a review of progress and evidence. *Nat Rev Gastroenterol Hepatol*. 2018;15(1):p. 39–49. doi:10.1038/nrgastro.2017.136
3. Mentella MC, Scaldaferri F, Pizzoferrato M, et al. Nutrition, IBD and gut microbiota: a review. *Nutrients*. 2020;12(4):4. doi:10.3390/nu12040944
4. Owczarek D, Rodacki T, Domagała-Rodacka R, et al. Diet and nutritional factors in inflammatory bowel diseases. *World J Gastroenterol*. 2016;22(3):p. 895–905. doi:10.3748/wjg.v22.i3.895
5. Kim IW, Myung S-J, Do MY, et al. Western-style diets induce macrophage infiltration and contribute to colitis-associated carcinogenesis. *J Gastroenterol Hepatol*. 2010;25(11):p. 1785–94. doi:10.1111/j.1440-1746.2010.06332.x
6. Okada Y, Tsuzuki Y, Sato H, et al. Trans fatty acids exacerbate dextran sodium sulphate-induced colitis by promoting the up-regulation of macrophage-derived proinflammatory cytokines involved in T helper 17 cell polarization. *Clin Exp Immunol*. 2013;174(3):p. 459–71. doi:10.1111/cei.12200
7. Gu MJ, Huang Q-C, Bao C-Z, et al. Attributable causes of colorectal cancer in China. *BMC Cancer*. 2018;18(1):p. 38. doi:10.1186/s12885-017-3968-z
8. Martinez-Useros J, Garcia-Foncillas J. Obesity and colorectal cancer: molecular features of adipose tissue. *J Transl Med*. 2016;14(p):21. doi:10.1186/s12967-016-0772-5
9. Kawai T, Autieri MV, Scalia R. Adipose tissue inflammation and metabolic dysfunction in obesity. *Am J Physiol Cell Physiol*. 2021;320(3):p. C375–c391. doi:10.1152/ajpcell.00379.2020
10. Saltiel AR, Olefsky JM. Inflammatory mechanisms linking obesity and metabolic disease. *J Clin Invest*. 2017;127(1):p. 1–4. doi:10.1172/JCI92035
11. Dixon SJ, Lemberg K, Lamprecht M, et al. Ferroptosis: an iron-dependent form of nonapoptotic cell death. *Cell*. 2012;149(5):p. 1060–72. doi:10.1016/j.cell.2012.03.042
12. Liu J, Kuang F, Kroemer G, et al. Autophagy-dependent ferroptosis: machinery and regulation. *Cell Chem Biol*. 2020;27(4):p. 420–435. doi:10.1016/j.chembiol.2020.02.005
13. Huang J, Zhang J, Ma J, et al. Inhibiting ferroptosis: a novel approach for ulcerative colitis therapeutics. *Oxid Med Cell Longev*. 2022;2022(p):9678625. doi:10.1155/2022/9678625
14. Xu S, He Y, Lin L, et al. The emerging role of ferroptosis in intestinal disease. *Cell Death Dis*. 2021;12(4):p. 289. doi:10.1038/s41419-021-03559-1
15. Xu J, Liu S, Cui Z, et al. Ferrostatin-1 alleviated TNBS induced colitis via the inhibition of ferroptosis. *Biochem Biophys Res Commun*. 2021;573(p):48–54. doi:10.1016/j.bbrc.2021.08.018
16. Wu Y, Ran L, Yang Y, et al. Deferasirox alleviates DSS-induced ulcerative colitis in mice by inhibiting ferroptosis and improving intestinal microbiota. *Life Sci*. 2023;314(p):121312. doi:10.1016/j.lfs.2022.121312
17. Yu Y, Yan Y, Niu F, et al. Ferroptosis: a cell death connecting oxidative stress, inflammation and cardiovascular diseases. *Cell Death Discov*. 2021;7(1):p. 193. doi:10.1038/s41420-021-00579-w
18. Galaris D, Barbouti A, Pantopoulos K. Iron homeostasis and oxidative stress: an intimate relationship. *Biochim Biophys Acta Mol Cell Res*. 2019;1866(12):p. 118535. doi:10.1016/j.bbamcr.2019.118535
19. Lee DH, Kim J-I, Lee MS, et al. Moxibustion for ulcerative colitis: a systematic review and meta-analysis. *BMC Gastroenterol*. 2010;10(p):36. doi:10.1186/1471-230X-10-36
20. Borovikova LV, Ivanova S, Zhang M, et al. Vagus nerve stimulation attenuates the systemic inflammatory response to endotoxin. *Nature*. 2000;405(6785):p. 458–62. doi:10.1038/35013070
21. Wei D, Zhao N, Xie L, et al. Electroacupuncture and moxibustion improved anxiety behavior in dss-induced colitis mice. *Gastroenterol Res Pract*. 2019; 2019: 2345890. doi:10.1155/2019/2345890
22. Kim HY, Hahm D-H, Pyun K-H, et al. Effects of acupuncture at GV01 on experimentally induced colitis in rats: possible involvement of the opioid system. *Jpn J Physiol*. 2005;55(3):p. 205–10. doi:10.2170/jjphysiol.S647
23. Song S, An J, Li Y, et al. Electroacupuncture at ST-36 ameliorates DSS-induced acute colitis via regulating macrophage polarization induced by suppressing NLRP3/IL-1β and promoting Nrf2/HO-1. *Mol Immunol*. 2019;106(p):143–152. doi:10.1016/j.molimm.2018.12.023

24. Zhu X, Liu Z, Niu W, et al. Effects of electroacupuncture at St25 and Bl25 in a Sennae-induced rat model of diarrhoea-predominant irritable bowel syndrome. *Acupunct Med*. 2017;35(3):p. 216–223. doi:10.1136/acupmed-2016-011180
25. Liu S, Wang Z, Su Y, et al. A neuroanatomical basis for electroacupuncture to drive the vagal-adrenal axis. *Nature*. 2021;598(7882):p. 641–645. doi:10.1038/s41586-021-04001-4
26. Xu MM, Guo Y, Chen Yet al. Electro-acupuncture promotes gut motility and alleviates functional constipation by regulating gut microbiota and increasing butyric acid generation in mice. *J Integr Med*. 2023;21(4):p. 397–406. doi:10.1016/j.joim.2023.05.003
27. Hirschhorn T, Stockwell BR. The development of the concept of ferroptosis. *Free Radic Biol Med*. 2019;133(p):130–143. doi:10.1016/j.freeradbiomed.2018.09.043
28. Seibt TM, Proneth B, Conrad M. Role of GPX4 in ferroptosis and its pharmacological implication. *Free Radic Biol Med*. 2019;133(p):144–152. doi:10.1016/j.freeradbiomed.2018.09.014
29. Kajarabille N, Latunde-Dada GO. Programmed cell-death by ferroptosis: antioxidants as mitigators. *Int J Mol Sci*. 2019;20(19):19. doi:10.3390/ijms20194968
30. Koppula P, Zhuang L, Gan B. Cystine transporter SLC7A11/xCT in cancer: ferroptosis, nutrient dependency, and cancer therapy. *Protein Cell*. 2021;12(8):p. 599–620. doi:10.1007/s13238-020-00789-5
31. Tian Y, Lu J, Hao X, et al. FTH1 inhibits ferroptosis through ferritinophagy in the 6-OHDA model of parkinson's disease. *Neurotherapeutics*. 2020;17(4):p. 1796–1812. doi:10.1007/s13311-020-00929-z
32. Iwa M, Matsushima M, Nakade Y, et al. Electroacupuncture at ST-36 accelerates colonic motility and transit in freely moving conscious rats. *Am J Physiol Gastrointest Liver Physiol*. 2006;290(2):p. G285–92. doi:10.1152/ajpgi.00068.2005
33. Jin H, Guo J, Liu J, et al. Anti-inflammatory effects and mechanisms of vagal nerve stimulation combined with electroacupuncture in a rodent model of TNBS-induced colitis. *Am J Physiol Gastrointest Liver Physiol*. 2017;313(3):p. G192–g202. doi:10.1152/ajpgi.00254.2016
34. Hu XF, Zhang H, Yu -L-L, et al. Electroacupuncture reduces anxiety associated with inflammatory bowel disease by acting on cannabinoid cb1 receptors in the ventral hippocampus in mice. *Front Pharmacol*. 2022;13(p):919553. doi:10.3389/fphar.2022.919553
35. Kim JH, Oh CM, Yoo JH. Obesity and novel management of inflammatory bowel disease. *World J Gastroenterol*. 2023;29(12):p. 1779–1794. doi:10.3748/wjg.v29.i12.1779
36. Yunita L, Viventius Y, Wahdini S. Case report: the role of multilead laser needle and laser pen with dietary interventions on grade 2 obesity. *Med Acupunct*. 2022;34(4):p. 266–270. doi:10.1089/acu.2022.0032
37. Carlos D, Pérez MM, Leite JA, et al. NOD2 deficiency promotes intestinal CD4+ T lymphocyte imbalance, metainflammation, and aggravates type 2 diabetes in murine model. *Front Immunol*. 2020;11(p):1265. doi:10.3389/fimmu.2020.01265
38. Song Y, Yuan M, Xu Y, et al. Tackling inflammatory bowel diseases: targeting proinflammatory cytokines and lymphocyte homing. *Pharmaceuticals (Basel*. 2022;15(9):9. doi:10.3390/ph15091080
39. Li X, Ren K, Hong X, et al. Ameliorating effects of electroacupuncture on the low-grade intestinal inflammation in rat model of diarrhea-predominant irritable bowel syndrome. *J Gastroenterol Hepatol*. 2022;37(10):p. 1963–1974. doi:10.1111/jgh.15981
40. Dodson M, Castro-Portuguez R, Zhang DD. NRF2 plays a critical role in mitigating lipid peroxidation and ferroptosis. *Redox Biol*. 2019;23(p):101107. doi:10.1016/j.redox.2019.101107
41. Zhou Z, Yang Z, Cui Y, et al. Identification and validation of a ferroptosis-related long non-coding RNA (FRlncRNA) signature to predict survival outcomes and the immune microenvironment in patients with clear cell renal cell carcinoma. *Front Genet*. 2022;13(p):787884. doi:10.3389/fgene.2022.787884
42. Huang F, Zhang S, Li X, et al. STAT3-mediated ferroptosis is involved in ulcerative colitis. *Free Radic Biol Med*. 2022;188(p):375–385. doi:10.1016/j.freeradbiomed.2022.06.242
43. Chen Y, Zhang P, Chen W, et al. Ferroptosis mediated DSS-induced ulcerative colitis associated with Nrf2/HO-1 signaling pathway. *Immunol Lett*. 2020;225(p):9–15. doi:10.1016/j.imlet.2020.06.005
44. Xu M, Tao J, Yang Y, et al. Ferroptosis involves in intestinal epithelial cell death in ulcerative colitis. *Cell Death Dis*. 2020;11(2):p. 86. doi:10.1038/s41419-020-2299-1
45. Luo L, Zhang S, Guo N, et al. ACSF2-mediated ferroptosis is involved in ulcerative colitis. *Life Sci*. 2023;313(p):121272. doi:10.1016/j.lfs.2022.121272
46. Cui DJ, Chen C, Yuan W-Q, et al. Integrative analysis of ferroptosis-related genes in ulcerative colitis. *J Int Med Res*. 2021;49(9):p. 3000605211042975. doi:10.1177/03000605211042975
47. Martin HL, Teismann P. Glutathione–a review on its role and significance in parkinson's disease. *FASEB j*. 2009;23(10):p. 3263–72. doi:10.1096/fj.08-125443
48. Gao W, Zhang T, Wu H. Emerging pathological engagement of ferroptosis in gut diseases. *Oxid Med Cell Longev*. 2021;2021(p):4246255. doi:10.1155/2021/4246255
49. Lei G, Mao C, Yan Y, et al. Ferroptosis, radiotherapy, and combination therapeutic strategies. *Protein Cell*. 2021;12(11):p. 836–857. doi:10.1007/s13238-021-00841-y
50. Feng H, Schorpp K, Jin J, et al. Transferrin receptor is a specific ferroptosis marker. *Cell Rep*. 2020; 30(10):p. 3411–3423. doi:10.1016/j.celrep.2020.02.049
51. Qiu P, Ishimoto T, Fu L, et al. The gut microbiota in inflammatory bowel disease. *Front Cell Infect Microbiol*. 2022;12(p):733992. doi:10.3389/fcimb.2022.733992
52. Jang JH, Yeom M-J, Ahn S, et al. Acupuncture inhibits neuroinflammation and gut microbial dysbiosis in a mouse model of Parkinson's disease. *Brain Behav Immun*. 2020;89(p):641–655. doi:10.1016/j.bbi.2020.08.015
53. Barbara G, Barbaro MR, Fuschi D, et al. Inflammatory and microbiota-related regulation of the intestinal epithelial barrier. *Front Nutr*. 2021;8(p):718356. doi:10.3389/fnut.2021.718356
54. Hu Y, Chen Z, Xu C, et al. Disturbances of the gut microbiota and microbiota-derived metabolites in inflammatory bowel disease. *Nutrients*. 2022;14(23):23. doi:10.3390/nu14235140